Proceedings of the 2002 IEEE
International Conference on Robotics & Automation
Washington, DC • May 2002

Singularity-Free Algorithms and Design Scheme for A New 6-DOF Parallel Haptic Device

Jae Hoon Lee, Hyung Wook Kim, Byung-Ju Yi, and Il Hong Suh
School of Electrical Engineering and Computer Science, Hanyang University, Korea
Email : bj@ hanyang.ac.kr

Abstract *It is known that parallel-type mechanisms have many singularities than serial-type mechanisms. In haptic application, these singularities deteriorate the system performance generating reflecting force. Moreover, different from general manipulators, haptic systems can't avoid the singular point, because they are operated by user's random command.*

Although many singularity-free algorithms for serial mechanisms have been proposed and studied, singularity-free algorithms for parallel haptic application have not been deeply discussed. In this paper, various singularity-free algorithms, which are appropriate to parallel haptic system, will be discussed. Furthermore, to overcome singularity problems, a new design including redundant actuation is proposed. The proposed mechanism has fairly large workspace and is relatively light by employing non-floating actuators.

Keywords : Haptic Device, Parallel Mechanism, Singularity, Redundant Actuation

1. Introduction

Since master-slave system proposed by Goertz in the 1950's[1], many researchers have developed various types of haptic display such as an exoskeleton type master arm by M. Bergamasco[5], PHANToM[3] by Massie and Salisbury, MagLev Wrist[4] by Hollis in CMU, and the magnetic levitation haptic interface by Merkelman et al [], etc.

Although many haptic interfaces have been developed as above, serial structures cannot achieve hard contact feeling. Other devices having parallel structure are heavy and have relatively small workspace, and require large power due to floating actuators[2,6-8].

To overcome these difficulties, new mechanism was proposed bye Gosselin [16] and Lee, et. al[14,15] which are light by employing non-floating and has relatively large workspace as compared to other parallel mechanisms.

Parallel mechanisms have many merits as haptic device in aspect of high structural stiffness, high force bandwidth, high force dynamic range, etc. However, it is known that parallel mechanisms have many singularities that deteriorate force reflection performance in haptic applications. At singular points, haptic system can't generate reflecting force completely, and moreover, actuator saturation happens. So singularity-free algorithms for maintaining system performance generating reflectng force need to be investigated.

Many singularity-free algorithms for serial mechanisms have been studied[9-13]. However, study on singularity-free algorithms for parallel-type haptic devices has been rare.

In this paper, various singularity-free algorithms for a new 6-DOF parallel haptic system are discussed and methods appropriate to a parallel haptic system are also suggested. Furthermore, as a new scheme to overcome these limitations, we propose a new design including redundant actuation.

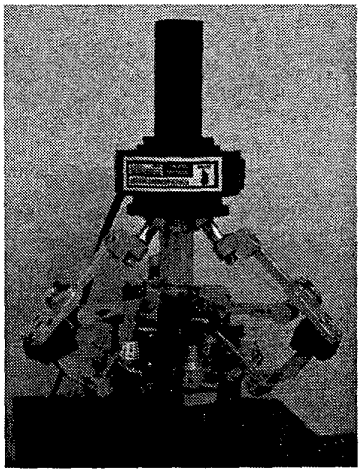

Fig. 1. New 6-DOF Parallel Haptic Device

2. Kinematics of 6-DOF Haptic Devices

2.1 Geometric Description

Fig 1. shows a new parallel-type haptic device. The proposed 6-DOF parallel haptic device consists of a top plate, six actuators on the base, and three parallel chains connecting the top plate to the six actuators.

To avoid interference between motor body and links, we placed upper actuators(M1) under the base plate by employing bevel gear sets displayed as right figure of Fig. 2. If actuating torque of upper actuator is transmitted to 1st joint through the bevel gear set, and l_1 is rotated. Fig. 3 is enlarged photograph of this new mechanism including bevel gear set. Because all actuators are placed under the base plate, this system has little interference between links and motors and the system has large workspace. Also, it looks very simple and smart.

In Fig. 4, let $\{B\}$ and $\{T\}$ be the base frame fixed to the ground with its origin at the center of the base and the local frame fixed to the top plate with its origin at the center of the top frame, respectively. Each of three ball-socket joints ($^m\underline{C}$,

$m = 1,2,3$) of the top plate is placed on the circle of radius (R_t) with 120° apart from each other. Three pairs of actuators are placed on the ground with 120° apart from each other. Each of three actuator pairs consists of the upper actuator (M1) that is placed on the circle of radius R_{B1} horizontally to the ground and the lower actuator (M2) that is placed on the circle of radius R_{B2} vertically to the ground. And H_B denotes the distance from upper actuator and lower actuator in the z-direction.

Each chain consists of upper closed-chain and lower closed-chain as Fig. 4. The upper chains connect the ball-socket joint ($^m\underline{C}$, $m = 1,2,3$) of the top plate to the upper actuator (M1).

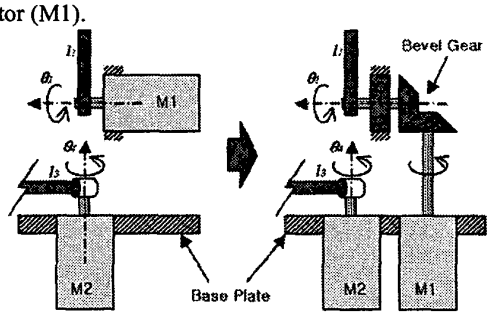

Fig. 2. Schematic Diagram of Bevel Gear Transmission

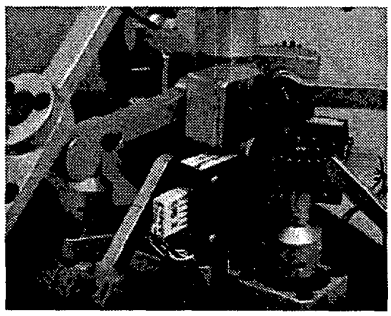

Fig. 3 Photograph of Bevel Gear Set

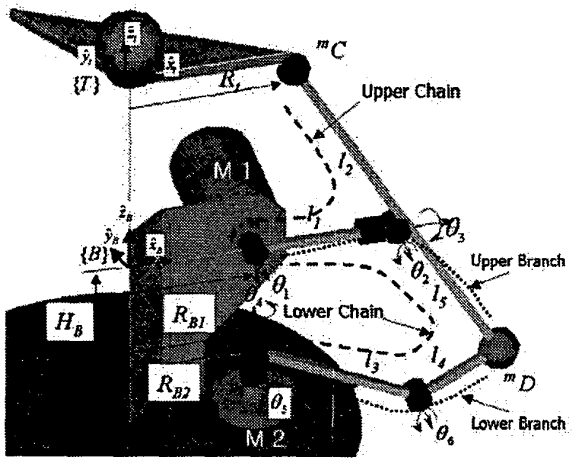

Fig. 4. Leg Structure of 6 DOF Parallel Haptic Device

And the lower chains connect the lower ball-socket joint ($^m\underline{D}$, $m = 1,2,3$) to the lower actuator (M2). Thus, structurally the upper actuators support gravity loads and generate the z-directional motion, and the lower actuators generate x-, and y-directional motions, respectively. Interaction of the three chains generates the rotational motion of the upper platform.

We define the output displacement vector as

$$\underline{u} = (x_t, y_t, z_t, \theta_x, \theta_y, \theta_z)^T, \quad (1)$$

where (x_t, y_t, z_t) represents the position of the origin of the top plate, and (θ_x, θ_y, θ_z) denotes $\hat{x}_t$ - $\hat{y}_t$ - $\hat{z}_t$ Euler angles equivalent to $[R_b^t]$ expressed by

$$[R_b^t] = [Rot(\hat{x}_t, \theta_x)]\,[Rot(\hat{y}_t, \theta_y)]\,[Rot(\hat{z}_t, \theta_z)] \quad . (2)$$

2.2 Forward/Inverse Kinematics

General parallel mechanisms have many forward kinematic solutions, and this new 6-DOF parallel haptic device has 8-th order polynomial. So we place 3 additional encoders at passive joints(θ_5) of lower chains to obtain a unique forward solution.

We can solve the inverse kinematic solution of each upper chain from the position vectors of the upper ball-socket joint ($^m\underline{C}$), which are given from the position and orientation of the top plate. In the same manner, the inverse kinematic solution of each lower chain can be obtained from position vectors of the lower ball-socket joint ($^m\underline{D}$, $m = 1,2,3.$), which are given from the forward kinematics of the upper chain.

2.3 First-order Kinematic Modeling

In the following, we describe the 1-*st* order KIC (Kinematic Influence Coefficient) as the relationship between the operational velocity ($\dot{\underline{u}}$) and the active joint velocity ($\dot{\underline{\theta}}_A$). Three upper contact points located at the upper ball-socket joints are denoted as

$$\underline{C} = ({}^1\underline{C}^T, {}^2\underline{C}^T, {}^3\underline{C}^T)^T, \quad (3)$$

where

$$^m\underline{C} = ({}^m_c x, {}^m_c y, {}^m_c z)^T. \quad (4)$$

Each upper contact point vector is expressed as

$$^m\underline{C} = \underline{u}_t + {}^m_c\underline{r}, \quad (5)$$

where

$${}^m_c\underline{r} = [R_b^t]\ {}^m_c\underline{r}^{(t)}. \quad (6)$$

Differentiating $^m\underline{C}$ with respect to time results in

$$^m\dot{\underline{C}} = \dot{\underline{u}}_t + \underline{\omega} \times {}^m_c\underline{r}, \quad (7)$$

where

$$\dot{\underline{u}}_t = (\dot{x}_t, \dot{y}_t, \dot{z}_t)^T, \quad (8)$$

$$\underline{\omega} = (\omega_x, \omega_y, \omega_z)^T, \quad (9)$$

and

$$ {}^{m}_{c}\underline{r} = ({}^{m}_{c}r_x, {}^{m}_{c}r_y, {}^{m}_{c}r_z)^T . \quad (10) $$

Eq. (7) can be written in a matrix form as

$$ {}^{m}\underline{\dot{C}} = [{}^{m}G^{c}_{u}]\,\underline{\dot{u}}, \quad (11) $$

where

$$ [{}^{m}G^{c}_{u}] = \begin{bmatrix} 1 & 0 & 0 & 0 & {}^{m}_{c}r_z & -{}^{m}_{c}r_y \\ 0 & 1 & 0 & -{}^{m}_{c}r_z & 0 & {}^{m}_{c}r_x \\ 0 & 0 & 1 & {}^{m}_{c}r_y & -{}^{m}_{c}r_x & 0 \end{bmatrix}, \quad (12) $$

$$ \underline{\dot{u}} = (\dot{x}_t, \dot{y}_t, \dot{z}_t, \omega_x, \omega_y, \omega_z)^T . \quad (13) $$

Then the relationship between $\underline{\dot{u}}$ and $\underline{\dot{C}}$ can be described as

$$ \underline{\dot{C}} = [G^{c}_{u}]\underline{\dot{u}}, \quad (14) $$

where

$$ [G^{c}_{u}] = \left[\; [{}^{1}G^{c}_{u}]^T [{}^{2}G^{c}_{u}]^T [{}^{3}G^{c}_{u}]^T \right]^T . \quad (15) $$

The open-chain kinematics of each leg is described as

$$ {}^{m}\underline{\dot{C}} = [{}^{m}_{u}G^{c}_{\theta}]\;{}^{m}_{u}\underline{\dot{\theta}}, \quad (16) $$

where ${}^{m}_{u}\underline{\dot{\theta}}$ is the joint velocity vector of the m-*th* upper chain.

Assuming no singularity in $[{}^{m}_{u}G^{c}_{\theta}]$, the first-order inverse kinematics of (16) is obtained as

$$ {}^{m}_{u}\underline{\dot{\theta}} = [{}^{m}_{u}G^{\theta}_{c}]\;{}^{m}\underline{\dot{C}} . \quad (17) $$

Congregating from $m = 1$ to 3 yields

$$ {}_{u}\underline{\dot{\theta}} = [{}_{u}G^{\theta}_{c}]\;\underline{\dot{C}} . \quad (18) $$

where

$$ {}_{u}\underline{\dot{\theta}} = ({}^{1}_{u}\underline{\dot{\theta}}^T \quad {}^{2}_{u}\underline{\dot{\theta}}^T \quad {}^{3}_{u}\underline{\dot{\theta}}^T)^T , $$

and

$$ [{}_{u}G^{\theta}_{c}] = \begin{bmatrix} [{}^{1}_{u}G^{\theta}_{c}] & 0 & 0 \\ 0 & [{}^{2}_{u}G^{\theta}_{c}] & 0 \\ 0 & 0 & [{}^{3}_{u}G^{\theta}_{c}] \end{bmatrix} . $$

2.4 Internal Kinematics

The lower closed chain consists of two branches which are constrained by the lower ball-socket joint (${}^{m}\underline{D}$, $m = 1 \sim 3$), and the common velocity at the lower ball-socket joint is described as

$$ {}^{m}\underline{\dot{D}} = [{}^{m}G^{D}_{u\theta}]\;{}^{m}_{u}\underline{\dot{\theta}} = [{}^{m}G^{D}_{l\theta}]\;{}^{m}_{l}\underline{\dot{\theta}} , \quad (19) $$

where $[{}^{m}G^{D}_{u\theta}]$ and $[{}^{m}G^{D}_{l\theta}]$ represent the 1-*st* order KICs for the upper branch and the lower branch, respectively. From Eq. (19), we can obtain the first-order kinematic relationship between the upper branch and the lower branch as

$$ {}^{m}_{l}\underline{\dot{\theta}} = [{}^{m}G^{D}_{l\theta}]^{-1}[{}^{m}G^{D}_{u\theta}]\;{}^{m}_{u}\underline{\dot{\theta}} = [{}^{m}G^{l\theta}_{u\theta}]\;{}^{m}_{u}\underline{\dot{\theta}}, \quad m = 1 \sim 3 . \quad (20) $$

Note that the active joints are ${}^{m}\dot{\theta}_1$ at the upper chain and ${}^{m}\dot{\theta}_4$ at the lower chain. Both actuators are located at the ground. By using a row-column selection of Eq. (20), the first-order relationship between the active joint velocity(${}^{m}\underline{\dot{\theta}}_A$: ${}^{m}\dot{\theta}_1$, ${}^{m}\dot{\theta}_4$, $m = 1 \sim 3$) and the joint velocity(${}_{u}\underline{\dot{\theta}}$) of the upper chains can be expressed as

$$ \underline{\dot{\theta}}_A = [G^{A}_{u\theta}]\;{}_{u}\underline{\dot{\theta}}, \quad (21) $$

where

$$ [G^{A}_{u\theta}] = \begin{bmatrix} 1\;0\;0 & \underline{0} & \underline{0} \\ [{}^{1}G^{l\theta}_{u\theta}]_{1;} & \underline{0} & \underline{0} \\ \underline{0} & 1\;0\;0 & \underline{0} \\ \underline{0} & [{}^{2}G^{l\theta}_{u\theta}]_{1;} & \underline{0} \\ \underline{0} & \underline{0} & 1\;0\;0 \\ \underline{0} & \underline{0} & [{}^{3}G^{l\theta}_{u\theta}]_{1;} \end{bmatrix}_{(6\times 9)} , \quad (22) $$

$$ {}_{u}\underline{\dot{\theta}} = [{}^{1}\theta_1\;{}^{1}\theta_2\;{}^{1}\theta_3\;{}^{2}\theta_1\;{}^{2}\theta_2\;{}^{2}\theta_3\;{}^{3}\theta_1\;{}^{3}\theta_2\;{}^{3}\theta_3]^T_{(9\times 1)} . \quad (23) $$

Substituting Eq. (17) into Eq. (21) yields the following relationship between the velocity of upper contact point the active joint velocity

$$ \underline{\dot{\theta}}_A = [G^{A}_{c}]\;\underline{\dot{C}} , \quad (24) $$

where

$$ [G^{A}_{c}] = [G^{A}_{u\theta}][{}_{u}G^{\theta}_{c}] . \quad (25) $$

And by substituting Eq. (14) into Eq. (24), the relationship between the operational velocity and active joint velocity is obtained as

$$ \underline{\dot{\theta}}_{A(6\times 1)} = [G^{A}_{u}]_{(6\times 6)}\underline{\dot{u}}_{(6\times 1)} \quad (26) $$

where

$$ [G^{A}_{u}] = [G^{A}_{c}][G^{c}_{u}] . \quad (27) $$

Assuming no singularity in $[G^{A}_{u}]$, the forward Jacobian is obtained by matrix inversion of $[G^{A}_{u}]$ as

$$ \underline{\dot{u}} = [G^{u}_{A}]\;\underline{\dot{\theta}}_A . \quad (28) $$

By duality relation, the relationship between the operational force and joint torque is described as

$$ \underline{T}_{u(6\times 1)} = [G^{A}_{u}]^T_{(6\times 6)}\underline{T}_{A(6\times 1)} . \quad (29) $$

where, $\underline{T}_{u(6\times 1)}$ and $\underline{T}_{A(6\times 1)}$ are the output force vector at the end-effector and the input torque vector required at active joints, respectively.

2.5 Kinematic Modeling of a 4-Legged 6-DOF Haptic Device

The kinematic structure of the proposed 4-Legged 6-DOF Haptic Device is the same as that of the 3-Legged Haptic system. This mechanism has 2 more actuators than system mobility, so it works in redundant actuation mode.

The 4-Legged 6-DOF Haptic Device consists of a top plate,

8 actuators on the base, and 4 parallel chains connecting the top plate to the 8 actuators displayed in Fig. 5. Each of four ball-socket joints (${}^{m}\underline{C}$, $m=1\sim4$.) of the top plate is placed on the circle of radius (R_t) with 90° apart from each other. Four pairs of actuators are placed on the ground with 90° apart from each other. Each of four actuator pairs consists of the upper actuator (M1) that is placed horizontal to the ground and the lower actuator (M2) that is placed vertical to the ground.

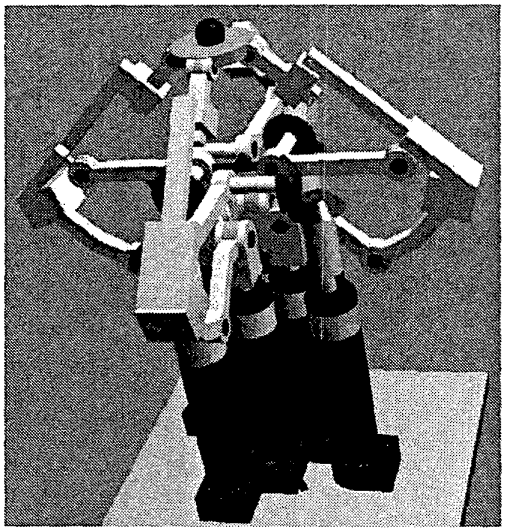

Fig. 5. 4-Legged 6-DOF Parallel Haptic Device

The forward/inverse kinematic solution and kinematic model of the 4-Legged Haptic device can be obtained as the same manner of the 3-Legged Haptic System, from Eq.(26) to Eq.(29). Consequently, the relationship between the operational velocity and active joint velocity is obtained as

$$\underline{\dot{\theta}}_{A(8\times1)} = [G_u^A]_{(8\times6)}\underline{\dot{u}}_{(6\times1)} \tag{30}$$

where

$$[G_u^A]_{(8\times6)} = [G_c^A]_{(8\times12)}[G_u^c]_{(12\times6)}. \tag{31}$$

And the relationship between the operational force and joint torque is described as

$$\underline{T}_{u(6\times1)} = [G_u^A]^T_{(6\times8)}\underline{T}_{A(8\times1)}. \tag{32}$$

3. Singularity-free Algorithms

General parallel mechanisms have some singular points in their workspace. Singularity causes serious problems such as torque saturation, undesirable motion, breakdown, etc. Several motion planning algorithms have been reported to avoid singularities of serial manipulators. However, parallel haptic devices cannot avoid singularity, because they are operated by the user's random command. Thus, singurlarity-free algorithms adequate to parallel haptic devices need to be investigated.

3.1 Singular Configurations

Fig. 6 shows three types of singularity of 3-Legged parallel haptic mechanism. Fig. 6 (a) shows the singularity that the top plate is parallel to one upper chain of legs. Fig. 6 (b) shows the singularity that the system touches the boundary of the workspace. Fig. 6 (c) shows an algorithmic singularity caused by internal kinematic problem.

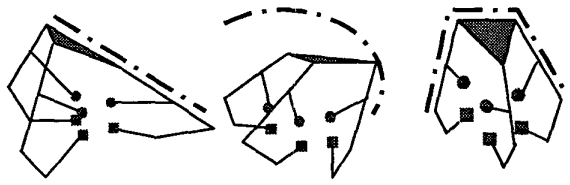

(a) (b) (c)

Fig. 6. Singular Configurations

3.2 Algorithm Near Singularity

This research work try to cope with the singularity problem of parallel haptic device by initially, using task-priority algorithm and damped lease-square method, and secondly, a new design employing redundant actuation.

The concept of task-priority algorithm was introduced by Maciejewski et al[10] and Nakamura et al[11] and applied to control of kinematically redundant manipulators. According to the task priority, the higher priority task is performed first and the lower priority task is performed sequentially by using the kinematic redundancy. In this paper, we reorganize this task-priority algorithm into force-priority algorithm for singularity problem in haptic system.

-Nakamura's algorithm

To begin with, consider Nakamura's algorithm for task priority redundancy resolution proposed in [11]. The subtask having the first priority will be specified using the first manipulation force, $\underline{T}_{u1} \in R^{m_1}$, and the secondary priority subtask will be specified using the second manipulation force, $\underline{T}_{u2} \in R^{m_2}$. From the Eq.(29), the force relationship between the joint torque $\underline{T}_A \in R^n$ and the output force vector is expressed as follows:

$$\begin{pmatrix}\underline{T}_{u1}\\ \underline{T}_{u2}\end{pmatrix} = \begin{bmatrix}J_1\\ J_2\end{bmatrix}\underline{T}_A = \begin{bmatrix}[G_u^A]_1^T\\ [G_u^A]_2^T\end{bmatrix}\underline{T}_A \tag{33}$$

where J_1 and J_2 are transposed Jacobian matrices for output force and moment, respectively. We chose the output force as the first priority task and the output moment as subtask in this work. However, we can reorganize the Jacobian matrices for other special applications.

The general solution of Eq. (33) for the first priority force is obtained using pseudoinverse as follows:

$$\underline{T}_A = J_1^+\underline{T}_{u1} + \{I - J_1^+J_1\}z \tag{34}$$

where the matrix J_1^+ is the pseudoinverse and z is the arbitrary vector that satisfies some secondary requirements. The m_2 -dimensional secondary task is specified by the following differential form

$$\underline{T}_{u2} = J_2 \underline{T}_A \in R^{m_2} \tag{35}$$

where $J_2 \in R^{m_2 \times n}$ is the Jacobian matrix for the secondary task. If we try to achieve the secondary task error $\|\underline{T}_{u2} - J_2 \underline{T}_A\|_2$ in the least square sense, then the least square solution z is obtained as follow [11]:

$$z = \left[J_2 \left\{ I - J_1^+ J_1 \right\} \right]^+ \left\{ \underline{T}_{u2} - J_2 J_1^+ \underline{T}_{u1} \right\} \tag{36}$$

Thus, the general solution of $\underline{T}_A$ is expressed as

$$\begin{aligned} \underline{T}_A &= J_1^+ \underline{T}_{u1} + \tilde{J}_2^+ \left\{ \underline{T}_{u2} - J_2 J_1^+ \underline{T}_{u1} \right\} \\ &\quad + \left\{ I - J_1^+ J_1 \right\} \left\{ I - \tilde{J}_2^+ \tilde{J}_2 \right\} z , \end{aligned} \tag{37}$$

where $\tilde{J}_2 = J_2 \left\{ I - J_1^+ J_1 \right\}$.

-Chiaverini's algorithm[12]

There are two kinds of singularities in solving inverse kinematics, in general. The one is the kinematic singularity and the other is algorithmic singularity [12]. The kinematic singularity occurs in the following case, and the latter case is called the secondary task singularity.

$rank(J_1) < m_1$ or $rank(J_2) < m_2$.

The algorithmic singularity occurs in either

$\Re(J_1^+) \cap \Re(J_2^+) \neq \phi$ when $m_2 \le n - m_1$ or

$\aleph(J_1) \cap \aleph(J_2) \neq \phi$ when $m_2 > n - m_1$ (38)

The kinematic singularity is the fundamental problem in solving the inverse kinematic, but the algorithmic singularity is an artificial part and can be eliminated or changed according to the characteristics of algorithm. Whatever the kinds of singularities, it should be noted that the general solution Eq.(37) is not acceptable near singularities.

To eliminate the algorithmic singularities existing in Nakamura's method, Chiaverini[12] modified Eq.(37) by as the following form

$$\underline{T}_A = J_1^+ \underline{T}_{u1} + \left\{ I - J_1^+ J_1 \right\} J_2^+ \underline{T}_{u2} + \left\{ I - J_1^+ J_1 \right\} \left\{ I - J_2^+ J_2 \right\} z \tag{39}$$

Although Nakamura's algorothm Eq.(37) has algorithmic singularities, the primary and the secondary tasks do not have any task error in the normal case. On the contrary, Chiaverini's algorithm Eq.(39) has no algorithmic singularity, but it always has the secondary task error except when $J_2 J_1^+ = 0$.

-Choi's algorithm[13]

By using the advantage that the Chiaverini's algorithm has no algorithmic singularity, Choi et al[13]proposed the algorithm that reduces the secondary task error of Eq.(39). The Chiaverini's algorithm can be modified to the following equation.

$$\underline{T}_A = J_W^+ \underline{T}_{u1} + \left\{ I - J_1^+ J_1 \right\} J_2^+ \underline{T}_{u2} + \left\{ I - J_1^+ J_1 \right\} \left\{ I - J_2^+ J_2 \right\} z \tag{40}$$

where $J_W^+ = W^{-1} J_1^T (J_1 W^{-1} J_1^T)^{-1}$. If the weight matrix is chosen to be positive definite matrix as follows

$$W = J_1^T J_1 + J_2^T J_2 + \varepsilon I > 0 \tag{41}$$

Then, Eq.(40) more of less contaminates the secondary task performance with small positive number ε, but has no algorithmic singularities.

-Damped Least Square Method

The singular value decomposition theorem states that for any matrix $A_{(m \times n)}$, there exist orthogonal matrices $U_{(m \times m)}$ and $V_{(n \times n)}$ such that

$$A = U \Sigma V^T \tag{42}$$

where, the matrx Σ has the block matrix form

$$\Sigma = \begin{bmatrix} S & \underline{0} \\ \underline{0} & \underline{0} \end{bmatrix}, \quad S = diag(\sigma_1, \cdots, \sigma_r), \quad r = rank(A) \tag{43}$$

Then, the pseudoinverse is given by

$$A^+ = V \Sigma^{-1} U^T, \Sigma = \begin{bmatrix} S^{-1} & \underline{0} \\ \underline{0} & \underline{0} \end{bmatrix}. \tag{44}$$

Wampler[9] initially proposed the damped least-square method, given by

$$A_\alpha^+ = V \Sigma_\alpha U^T . \tag{45}$$

where the $n \times m$ matrix Σ_α is

$$\Sigma_\alpha = \begin{bmatrix} S_\alpha \\ \underline{0} \end{bmatrix}, S_\alpha = diag\left(\frac{\sigma_1}{\sigma_1^2 + \alpha^2}, \cdots, \frac{\sigma_m}{\sigma_m^2 + \alpha^2} \right). \tag{46}$$

If α is much less than the smallest nonzero singular value of J, then $\underline{T}_{A\alpha}$ is minimum norm, least-square solution $\underline{T}_{A0}$. As a singular value approaches zero, the associated component of S_α reaches a maximum when $\sigma = \alpha$ and then decreases rapidly to zero. The size of the solution, $\|\underline{T}_\alpha\|$, decreases monotonically as α increases. This is useful fact that can be exploited to find solutions subject to joint torque limits.

4. Simulation

At a singular point, the parallel haptic system cannot generate desired 6-DOF force/moment completely. Moreover, torque saturation happens in singular points. Therefore, for stable and precise manipulation, though less important tasks cannot be obtained fully, some more important tasks have to be maintained without torque saturation. The user can choose task priority according to special purpose and condition. In this paper, we set 3-DOF force and 3-DOF moment as the first and the second priority task, respectively.

We investigated the performance of several singularity-free algorithms near singularity. The actuator torques are computed by various algorithms, and the output force/moment are simulated.

Table 1 through Table 3 show the simulation results of 3-Legged Parallel Haptic Device. Table 1 includes the

simulation result when the system is in a nonsingular position. The results of Inverse Jacobian, Nakamura's, and SVD Damping method are almost the same and satisfactory. However, the Chiaverini's and Choi's algorithms cannot fully generate the second priority task(i.e., moment).

Table 2 shows the simulation result when the system is in a singular position given by Fig. 6(a). When the pitch angle of the top plate is given *43.94* deg, the first chain and the top plate are parallel. The actuator torques of Inverse Jacobian and Nakamura's algorithms are saturated. However, Chiaverini's, Choi's and SVD Damping algorithm guarantee the first priority task(i.e., force).

Table 3 shows the simulation result when the system is in a singular position given by Fig. 6(b). Like as Table 2, Chiaverini's, Choi's and Damping algorithm guarantee the first priority task(force). However, the actuator torques of Inverse Jacobian and Nakamura's algorithms are saturated.

Table 4 is the simulation results of 4-Legged Parallel Haptic Device with redundant actuation. Actuator saturation cannot be found in every algorithm. However, Chiaverini's and Choi's methods have some output force/torque errors.

The variation of the 2-norm of actuator torque vector near the singularity is displayed in Fig. 7. The torque norms of Inverse Jacobian and Nakemura's methods increase exponentially as approaching to a singular point and the norms of Chiaverini's and Choi's methods are too small because the output moment cannot be fully achieved. However, the torque norm of damping method decreases near a singular point.

Table 1. Comparison of Singularity-free Algorithms (nonsingular position)

Boldface number : Actuator Torque

Italic number : Output Force/Moment

Position	X (cm)	Y (cm)	Z (cm)	Roll (Deg)	Pitch (Deg)	Yaw (Deg)
	0.0	0.0	10.0	0.0	0.0	0.0
Desired Force	5.0 (N)	5.0 (N)	0.0 (N)	0.5 (Nm)	0.5 (Nm)	0.0 (Nm)
Method	Actuator Torque(Nm)					
	Output Force(N)			*Output Moment(Nm)*		
Inverse Jacobian	-3.958	-5.035	3.122	-6.376	0.836	6.376
	5.0	*5.0*	*0.0*	*0.5*	*0.5*	*0.0*
Nakamura	-3.958	-5.035	3.122	-6.376	0.836	6.376
	5.0	*5.0*	*0.0*	*0.5*	*0.5*	*0.0*
Chiaverini	-0.513	-0.568	0.224	0.018	0.289	0.649
	5.0	*5.0*	*0.0*	*-0.014*	*0.065*	*-0.066*
Choi	-0.527	-0.669	0.270	0.03	0.257	0.71
	5.0	*5.0*	*0.0*	*0.003*	*0.067*	*-0.073*
SVD Damping	-3.788	-4.986	3.026	-6.065	0.762	9.09
	5.0	*4.999*	*0.0*	*0.495*	*0.479*	*-0.003*

Table 2. Comparison of Singularity-free Algorithms (Fig. 4(a) configuration)

Boldface number : Actuator Torque

Italic number : Output Force/Moment

Position	X (cm)	Y (cm)	Z (cm)	Roll (Deg)	Pitch (Deg)	Yaw (Deg)
	0.0	0.0	10.0	0.0	43.94	0.0
Desired Force	5.0	5.0	0.0	0.5	0.5	0.0
Method	Actuator Torque(Nm)					
	Output Force(N)			*Output Moment(Nm)*		
Inverse Jacobian	-98655	-4.565	47822.2	-188204	47820.4	188203.
	5.0	*5.0*	*0.0*	*0.5*	*0.5*	*0.0*
Nakamura	-98655	-4.565	47822.2	-188204	47820.4	188203.
	4.999	*4.999*	*0.0*	*0.5*	*4.999*	*0.0*
Chiaverini	-0.242	-0.488	-0.044	0.146	0.269	-0.039
	5.0	*5.0*	*0.0*	*-0.0885*	*0.0347*	*0.0*
Choi	-0.242	-0.629	0.015	0.206	0.209	0.021
	5.0	*5.0*	*0.0*	*-0.058*	*0.035*	*-0.016*
SVD Damping	-0.245	-4.529	0.993	-0.183	-0.766	-0.358
	5.003	*4.999*	*0.003*	*0.497*	*0.035*	*-0.002*

Table 3. Comparison of Singularity-free Algorithms (boundary singular position: Fig. 4 (b))

Boldface number : Actuator Torque

Italic number : Output Force/Moment

Position	X (cm)	Y (cm)	Z (cm)	Roll (Deg)	Pitch (Deg)	Yaw (Deg)
	8.56	0.0	10.0	0.0	0.0	0.0
Desired Force	5.0	5.0	0.0	0.5	0.5	0.0
Method	Actuator Torque(Nm)					
	Output Force(N)			*Output Moment(Nm)*		
Inverse Jacobian	-2.781	5.741	-13.94	7.37	0.895	0.45
	5.0	*5.0*	*0.0*	*0.5*	*0.5*	*0.0*
Nakamura	-2.781	5.741	-13.94	7.37	0.895	0.45
	5.0	*5.0*	*0.0*	*0.5*	*0.5*	*0.0*
Chiaverini	-0.145	1.101	-7.33	3.79	7.56	3.913
	5.0	*5.0*	*0.0*	*-0.90*	*0.023*	*2.843*
Choi	-0.155	2.083	-6.71	3.50	6.89	3.592
	5.0	*5.0*	*0.0*	*-0.31*	*0.03*	*1.567*
SVD Damping	-1.294	1.608	-5.15	2.73	-0.40	-0.22
	5.0	*5.0*	*0.0*	*0.22*	*0.23*	*0.128*

Table 4. Comparison of Singularity-free Algorithms (4-Legged Haptic System)

Boldface number : Actuator Torque

Italic number : Output Force/Moment

Position	X (cm)	Y (cm)	Z (cm)	Roll (Deg)	Pitch (Deg)	Yaw (Deg)
	0.0	0.0	10.0	0.0	43.94	0.0
Desired Force	5.0	5.0	0.0	0.5	0.5	0.0
Method	Actuator Torque(Nm)					
	Output Force(N)			*Output Moment(Nm)*		
Inverse Jacobian	0.379	-0.572	-0.159	0.448	-0.430	0.465
	5.0	*5.0*	*0.0*	*0.5*	*0.5*	*0.0*
Nakamura	0.379	-0.572	-0.159	0.448	-0.430	0.465
	5.0	*5.0*	*0.0*	*0.5*	*0.5*	*0.0*
Chiaverini	0.454	-0.432	-0.077	0.447	-0.510	0.560
	5.0	*5.0*	*0.0*	*0.278*	*0.638*	*-1.185*
Choi	0.401	-0.558	-0.142	0.436	-0.451	0.473
	5.0	*5.0*	*0.0*	*0.4735*	*0.549*	*-0.008*
SVD Damping	0.379	-0.572	-0.159	0.448	-0.430	0.465
	5.0	*5.0*	*0.0*	*0.5*	*0.5*	*0.0*

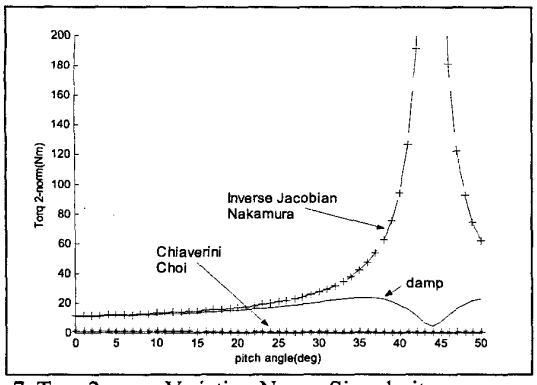

Fig. 7. Torq 2-norm Variation Near a Singularity

From the simulation results described above, we could draw some conclusions, as follow.

(1) Inverse jacobian algorithm is not applicable to force reflection because of actuator torque saturation at near singularities.

(2) Task-priority method such as Chiaverini's and Choi's algorithm did not cause actuator torque saturation at singularities. However, they cannot guarantee second priority task even in nonsingular workspace. So these methods did not suit to haptic application.

(3) Damped Least Square algorithm guarantees first priority tasks in not only singular points but also nonsingular workspace. And it did not cause actuator torque saturation at singular positions. Thus, it can be used as the most stable singularity-free algorithm.

(4) New design including redundant actuation can reduce singularities in parallel haptic system dramatically. Thus, redundant actuation can be suggested as a good solution to singularity-free haptic design.

5. Conclusion

In this paper, we tested various singularity-free algorithms for operation of parallel haptic device. We could observe that many task-priority algorithms developed for resolution of kinematic redundancy are not appropriate to haptic application using parallel device.

Damped least-square method has the best performance near singular positions. And a new design including redundant actuation is proposed. The proposed new mechanism has singularity-free structure owing to redundant actuation. And it is relatively light by employing non-floating actuators and has large workspace. Redundant actuation can be suggested as a good solution to singularity-free haptic design.

As a further study, experiments testing performances of singularity-free algorithms are now ongoing.

Acknowledgment

This work was supported by grant No. R01-2000-00260 from the Korea Science & Engineering Foundation.

Reference

[1] R.C. Goertz, "Fundamentals of General-Purpose Remote Manipulators," Journal of Nucleonics, Vol. 10, No. 11, pp.36-42, 1952.

[2] R.E. Ellis, O.M. Ismaeil, and M.G. Lipsett, "Design and Evaluation of High-Performance Haptic Interface", Robotica, Vol.4., 1996.

[3] T. Massie, K. Stalisbury, "PHANToM Haptic Interface: A Device for Probing Virtual Objects", ASME Journal of Dynamic System and Control, New York, NY, pp.295-299, 1994.

[4] P. J. Berkelman, R. L. Hollis, and S. E. Salcudean, "Interacting with Virtual Environments using a Magnetic Levitation Haptic Interface", Proceedings of IEEE International Conference on Intelligent Robots and Systems, pp. 117-122, piscataway, NJ, 1995.

[5] M. Bergamasco, et al., "An Arm Exoskeleton System for Teleoperation and Virtual Environments Applications," Proceedings of International Conference On Robotics and Automation, San Diego, California, pp. 1449-1454, 1994.

[6] M. Ishii and M. Sato, "A 3D Spatial Interface Device Using Tensed Strings," Presence-Teleoperators and Virtual Environments, Vol.3, No.1, MIT Press, Cambridge, MA, pp.81-86, 1994.

[7] J.M. Hollerbarch, "Some Current Issues in Haptic Research," Proceedings of International Conference On Robotics and Automation, pp. 757-762, 2000.

[8] J.H. Lee, B-J. Yi and S.R. Oh, "Optimal Design of a Five-Bar Finger with Redundant Actuation," Proceedings of International Conference On Robotics and Automation, pp. 2068-2074, 1998.

[9] Charles W. Wampler, "Manipulator Inverse Kinematic Solutions Based on Vector Formulations and Damped Least-Squares Methods," IEEE Transactions on System, Man, Cybernetics, Vol. SMC-16, No. 1, 1986.

[10] A. A. Maciejewski and C. A. Klein, "Obstacle Avoidnace for Kinematically Redundant Manipulators in Dynamically Varying Environments," International Journal of Robotics Research, Vol.4, No.3, pp.109-117, 1985.

[11] Y. Nakamura, H. Hanafusa and T. Yoshikawa, "Task-Priority based Redundancy Control of Robot Manipulators," International Journal of Robotics Research, Vol.6, No.2, pp.3-15, 1987.

[12] S. Chiaverini, "Singularity-robust Task-priority Redundancy Resolution for Real-time Kinematic Control of Robot Manipulators," IEEE Trans. On Robotics and Automation, Vol.13, No.3, pp.398-410, 1997.

[13] Y. J. Choi, W. K. Chung, Y. W. Oh, S. R. Oh and I. H. Suh, "On the Task Priority Manipulation Scheme with High Execution Performance for a Robotic Manipulator," International Conference On Advanced Robotics, 2001.

[14] Lee, J.H., Eom, K.S, Yi, B-J. and Suh, I.H., "Design Of A New 6-DOF Parallel Haptic Device," Proceedings of International Conference On Robotics and Automation, pp. 886-891, 2001.

[15] Kim, H.W., Eom, K.S, Suh, I.H. and Yi, B-J., "A Transparency-optimized Control for a New 6-DOF Parallel-structured Haptic Device," Proceedings of International Conference On Robotics and Automation, pp. 2331-2336, 2001.

[16] Gosselin, C.M., Allan, J.F., and Lalibert, T., "A New Architecture for a High-performance 6-DOF Parallel Mechanism," Proceeding of the IFToMM Tenth World Congress on the Theory of Machine and Mechanisms, Oulu, Finland, 20-24 June, pp. 1140-1145, 1999.